

Horizon structure of rotating Einstein-Born-Infeld black holes and shadow

Farruh Atamurotov^{a,1,2}, Sushant G. Ghosh^{b,3,4}, Bobomurat Ahmedov^{c,1,5},

¹Institute of Nuclear Physics, Ulughbek, Tashkent 100214, Uzbekistan

²Inha University in Tashkent, Tashkent 100170, Uzbekistan

³Centre for Theoretical Physics, Jamia Millia Islamia, New Delhi 110025, India

⁴Astrophysics and Cosmology Research Unit, School of Mathematical Sciences, University of Kwa-Zulu-Natal, Private Bag 54001, Durban 4000, South Africa

⁵Ulugh Beg Astronomical Institute, Astronomicheskaya 33, Tashkent 100052, Uzbekistan

the date of receipt and acceptance should be inserted later

Abstract We investigate the horizon structure of the rotating Einstein-Born-Infeld solution which goes over to the Einstein-Maxwell's Kerr-Newman solution as the Born-Infeld parameter goes to infinity ($\beta \rightarrow \infty$). We find that for a given β , mass M and charge Q , there exist critical spinning parameter a_E and r_H^E , which corresponds to an extremal Einstein-Born-Infeld black hole with degenerate horizons, and a_E decreases and r_H^E increases with increase in the Born-Infeld parameter β . While $a < a_E$ describe a non-extremal Einstein-Born-Infeld black hole with outer and inner horizons. Similarly, the effect of β on infinite redshift surface and in turn on ergoregion is also included. It is well known that a black hole can cast a shadow as an optical appearance due to its strong gravitational field. We also investigate the shadow cast by the non-rotating ($a = 0$) Einstein-Born-Infeld black hole and demonstrate that the null geodesic equations can be integrated that allows us to investigate the shadow cast by a black hole which is found to be a dark zone covered by a circle. Interestingly, the shadow of the Einstein-Born-Infeld black hole is slightly smaller than for the Reissner-Nordstrom black hole. Further, the shadow is concentric circles whose radius decreases with increase in value of parameter β .

1 Introduction

In Maxwell's electromagnetic field theory, the field of a point-like charge is singular at the charge position and hence it has infinite self-energy. To overcome this prob-

lem in classical electrodynamics, the non-linear electromagnetic field has been proposed by Born and Infeld [1], with main motivation, to resolve self-energy problem by imposing a maximum strength of the electromagnetic field. In this theory the electric field of a point charge is regular at the origin and this non-linear theory for the electromagnetic field was able to tone down the infinite self energy of the point-like charged particle. Later, Hoffmann [2] coupled has general relativity with Born-Infeld electrodynamics to obtain a spherically symmetric solutions for the gravitational field of an electrically charged object. Remarkably, after a long discard, the Born-Infeld theory made a come back to the stage in the context of more modern developments, which is mainly due to the interest in non-linear electrodynamics in the context of low energy string theory, in which Born-Infeld type actions appeared [3]. Indeed, the low energy effective action in an open superstring in loop calculations lead to Born-Infeld type actions [4]. These important features of the Born-Infeld theory, together with its corrective properties concerning singularities, further motivate to search for gravitational analogues of this theory in the past [5], and also interesting measures have been taken to get the spherically symmetric solutions [6]. The thermodynamic properties and causal structure of the Einstein-Born-Infeld black holes drastically differ from that of the classical Reissner-Nordstrom black holes. Indeed, it turns out that the Einstein-Born-Infeld black hole singularity is weaker than that of Reissner-Nordstrom black hole. Further properties of these black holes, including motion of the test particles has been also addressed [7]. It is worthwhile to mention that Kerr [8] and Kerr-Newman metrics [9] are undoubtedly the most significant exact solutions in the general relativity, which represent ro-

^ae-mail: farruh@astrin.uz, fatamurotov@gmail.com

^be-mail: sghosh2@jmi.ac.in, sghosh@gmail.com

^ce-mail: ahmedov@astrin.uz

tating black hole that can arise as the final fate of gravitational collapse. The generalization of the spherically symmetric Einstein-Born-Infeld black hole in the rotating case, Kerr-Newman like solution, was studied by Lombardo [10]. In particular, it is demonstrated [1] that the rotating Einstein-Born-Infeld solutions can be derived starting from the corresponding exact spherically symmetric solutions [2] by a complex coordinate transformation previously developed by Newman and Janis [9]. The rotating Einstein-Born-Infeld black hole metrics are axisymmetric, asymptotically flat and depend on the mass, charge and spin of the black hole as well as on a Born-Infeld parameter (β) that measure potential deviations from the Kerr metric Kerr-Newman metrics. The rotating Einstein-Born-Infeld metric includes the Kerr-Newman metric as the special case if this deviation parameter diverges ($\beta \rightarrow \infty$) as well as the Kerr metric when this parameter vanishes ($\beta = 0$). In this paper, we carry out detailed analysis of the horizon structure of rotating Einstein-Born-Infeld black hole and explicitly manifest the impact that the parameter β makes. Recently, horizon structure has been studied for various space-time geometris, see, e.g., [11]. We also investigate the apparent shape of non-rotating Einstein-Born-Infeld black hole to visualize the shape of the shadow and compare the results with the images for the corresponding Reissner-Nordstrom black hole. In spite of the fact that's a black hole is invisible, its shadow can be observed if it is in front of a bright background [12] as the result of the gravitational lensing effect, see, e.g., [14,13]. The photons that cross the event horizon, due to strong gravity, are removed from the observable universe which lead to a shadow (silhouette) imprinted by a black hole on the bright emission that exists in its vicinity. So far the shadow of the compact gravitational objects in the different cases have been extensively studied, see, e.g., [15]. Furthermore new general formalism to describe the shadow of black hole as an arbitrary polar curve expressed in terms of a Legendre expansion is developed in the recent paper [16]. The organization of the paper is as follows: In the Section II, we study the structure and location of an event horizon and the infinite redshift surface of the rotating Einstein-Born-Infeld black holes. We have also discussed the particle motion around the rotating Born-Infeld black hole in the Section II that helped us to investigate the shadow of the black hole in the Section III. In Section IV emission energy is analysed of rotating Einstein-Born-Infeld black holes. Finally, in Section V, we conclude by summarizing the main results. We use units which fix the speed of light and the gravitational constant via $G = c = 1$, and use the metric signature $(-, +, +, +)$.

2 Rotating Einstein-Born-Infeld black hole

The action for the gravitational field coupled to a non-linear Born-Infeld electrodynamics (or a Einstein-Born-Infeld action) in $(3 + 1)$ dimensions reads [1,2]

$$S = \int d^4x \sqrt{-g} \left[\frac{R}{16\pi G} + \mathcal{L}(\mathcal{F}) \right], \quad (1)$$

where R is scalar curvature, $g \equiv \det |g_{\mu\nu}|$ and $\mathcal{L}(\mathcal{F})$ is given by

$$\mathcal{L}(\mathcal{F}) = \frac{\beta^2}{4\pi G} \left(1 - \sqrt{1 + \frac{2\mathcal{F}}{\beta^2}} \right), \quad (2)$$

with $\mathcal{F} = \frac{1}{4} F_{\mu\nu} F^{\mu\nu}$, $F_{\mu\nu}$ denotes the electromagnetic field tensor. Here β^2 is the Born-Infeld parameter being equal to the maximum value of electromagnetic field intensity and has a dimension of $[length]^{-2}$. Eq. (1) leads to the Einstein field equations

$$R_{\mu\nu} - \frac{1}{2} g_{\mu\nu} R = \kappa T_{\mu\nu}, \quad (3)$$

and electromagnetic field equation

$$\nabla_{\mu} (F^{\mu\nu} \mathcal{L}_{,\mathcal{F}}) = 0. \quad (4)$$

The energy momentum tensor is

$$T_{\mu\nu} = \mathcal{L} g_{\mu\nu} - F_{\mu\sigma} F_{\nu}^{\sigma}, \quad (5)$$

where $\mathcal{L}_{,\mathcal{F}}$ denotes partial derivative of \mathcal{L} with respect to \mathcal{F} .

The gravitational field of a static and spherically symmetric compact object with mass M and a non-linear electromagnetic source in the Einstein-Born-Infeld theory has first been investigated by Hoffmann [2] and the space-time metric is [2,17]

$$ds^2 = - \left[1 - \frac{2GM}{r} + \frac{Q^2(r)}{r^2} \right] dt^2 + \left[1 - \frac{2GM}{r} + \frac{Q^2(r)}{r^2} \right]^{-1} dr^2 + r^2 (d\theta^2 + \sin^2 \theta d\varphi^2), \quad (6)$$

with the square of electric charge

$$Q^2(r) = \frac{2\beta^2 r^4}{3} \left(1 - \sqrt{1 + \zeta^2(r)} \right) + \frac{4Q^2}{3} F \left(\frac{1}{4}, \frac{1}{2}, \frac{5}{4}, -\zeta^2(r) \right), \quad (7)$$

where F is a Gauss hypergeometric function [18] and new notation $\zeta^2(r) = Q^2/(\beta^2 r^4)$ is introduced. From the radial dependence of $Q^2(r)$ plotted in Fig.1 one can see its strong dependence from β parameter near to the center of the black hole. The rotating counterpart of the Einstein-Born-Infeld black hole has been obtained in [10]. The gravitational field of rotating Einstein-Born-Infeld black hole spacetime is described by the metric

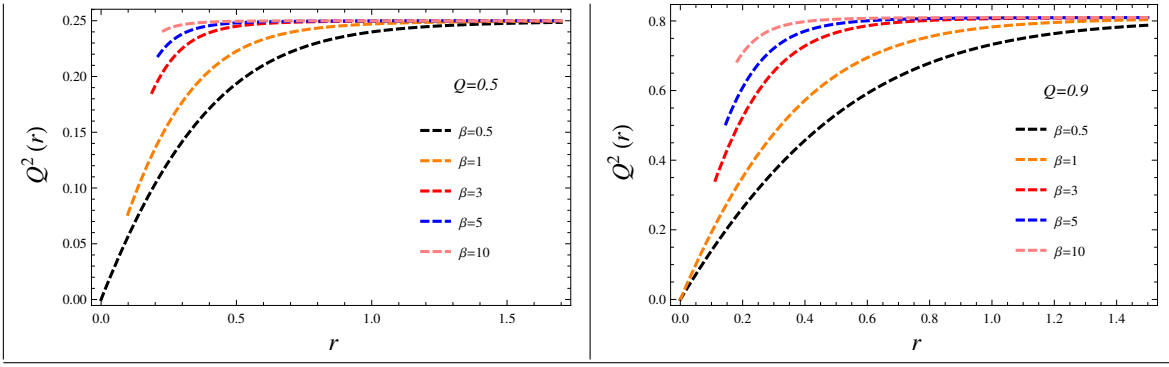


Fig. 1 Plots showing the dependence of the square of the electric charge $Q^2(r)$ from the radial coordinate r for different values of Born-Infeld parameter β . Left panel is for $Q = 0.5$ and right panel is for $Q = 0.9$ in asymptotics.

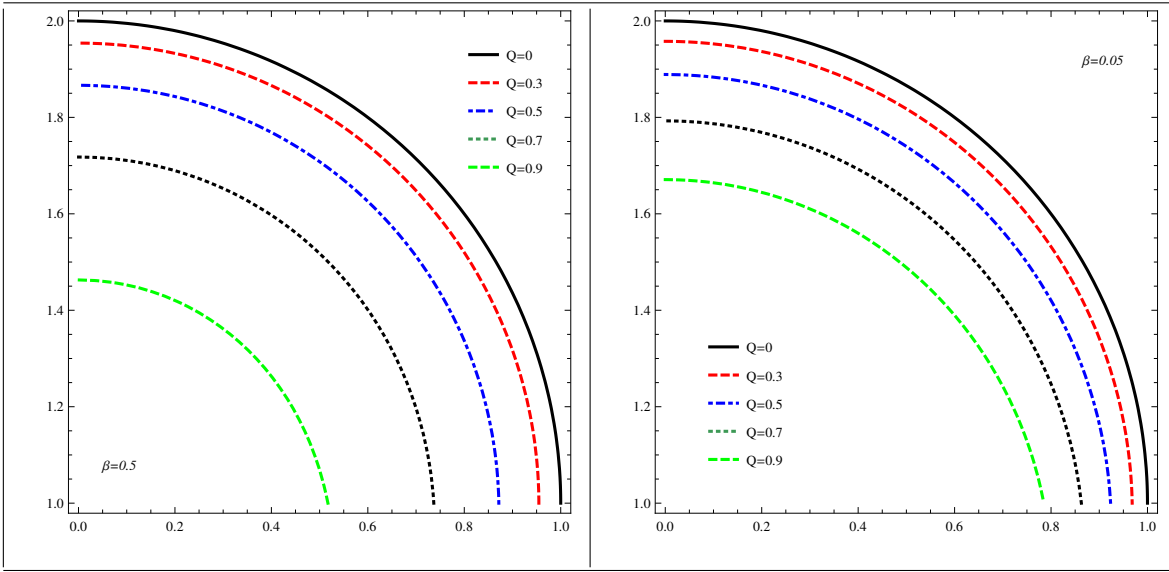


Fig. 2 The rotation parameter a dependence of the radial coordinate r for the different value of electric charge Q and Born-Infeld parameter β . The lines separate the region of black holes with naked singularity ones. The left panel is for Born-Infeld parameter $\beta = 0.5$ and the right panel is for Born-Infeld parameter $\beta = 0.05$.

which in the Boyer-Lindquist coordinates is given by [10]

$$\begin{aligned}
 ds^2 = & \frac{\Delta - a^2 \sin^2 \theta}{\rho^2} dt^2 - \frac{\rho^2}{\Delta} dr^2 \\
 & + 2a \sin^2 \theta \left(1 - \frac{\Delta - a^2 \sin^2 \theta}{\rho^2} \right) dt d\phi - \rho^2 d\theta^2 \\
 & - \sin^2 \theta \left[\rho^2 + a^2 \sin^2 \theta \left(2 - \frac{\Delta - a^2 \sin^2 \theta}{\rho^2} \right) \right] d\phi^2, \quad (8)
 \end{aligned}$$

with

$$\Delta = r^2 - 2GMr + Q^2(r) + a^2, \text{ and } \rho^2 = r^2 + a^2 \cos^2 \theta. \quad (9)$$

The parameters a , M , Q and β are, respectively correspond to rotation, mass, the electric charge and the Born-Infeld parameter. We let the parameters Q and β to be positive. In the limit $\beta \rightarrow \infty$ (or $Q(r) =$

Q) and $Q \neq 0$, one obtains the corresponding solution for Kerr-Newman black hole, while one has Kerr black hole [8] when $\beta \rightarrow 0$. The metric (8) is a rotating charged black hole which generalizes the standard Kerr-Newman black hole and we call it as the rotating Einstein-Born-Infeld black hole. The non-rotating case, $a = 0$, corresponds to the metric of the static Einstein-Born-Infeld black hole obtained by Hoffmann in [2]. The metric (8) has curvature singularity at the set of points, where $\rho = 0$ and $M = Q \neq 0$. For $a \neq 0$, it corresponds to a ring with radius a , in the equatorial plane $\theta = \pi/2$ and hence termed as a ring singularity. The properties of the rotating Einstein-Born-Infeld metric (8) are similar to that of the general relativity counterpart Kerr-Newman black hole. We first show that, it is possible to get certain range of values of a , M and Q , the metric (8) is a black hole. The metric (8), like

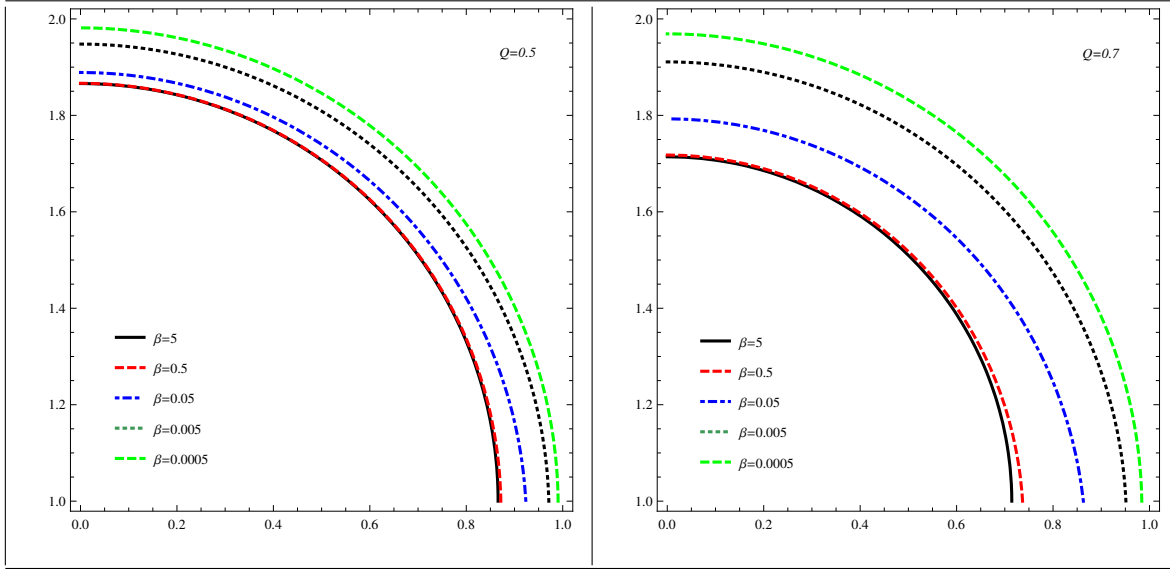


Fig. 3 The rotation parameter a dependence of the radial coordinate r for the different value of electric charge Q and Born-Infeld parameter β . The lines separate the region of black holes with naked singularity ones. The left panel is for electric charge $Q = 0.5$ and the right panel is for electric charge $Q = 0.7$.

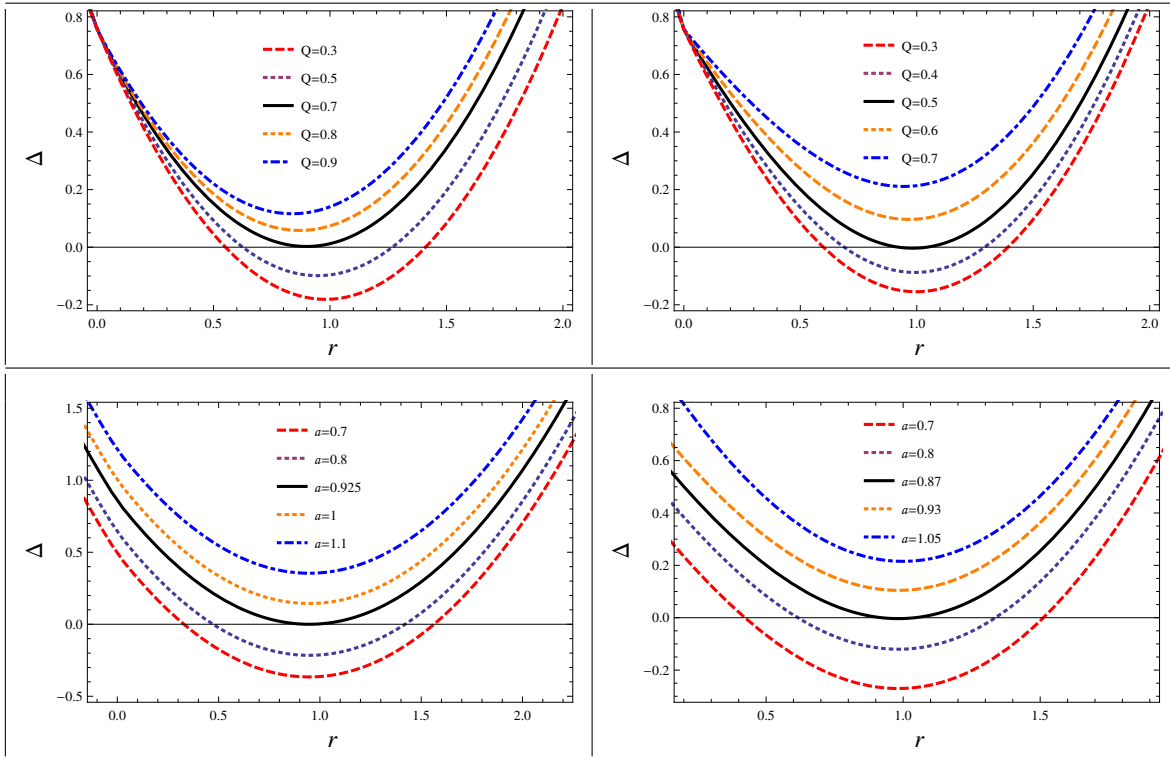


Fig. 4 Plots showing the radial dependence of Δ for the different values of Born-Infeld parameter β , electric charge Q and rotation parameter a (with $M = 1$). Top, left panel is for $a = 0.87$ and $\beta = 0.05$. Top, right panel is for $a = 0.87$ and $\beta = 0.5$. Bottom, left panel is for $Q = 0.5$ and $\beta = 0.05$. Bottom, right panel is for $Q = 0.5$ and $\beta = 0.5$.

the Kerr-Newman one, is singular at $\Delta = 0$ and it admits two horizons like surfaces, viz., the static limit surface and the event horizon. Here, we shall look for these two surfaces for the rotating Einstein-Born-Infeld metric (8) and discuss effect of the nonlinear parameter β . The horizons of the Einstein-Born-Infeld black hole (8) are dependent on parameters M, a, Q and β , and are calculated by equating the g^{rr} component of the metric (8) to zero, i.e.,

$$\Delta = r^2 - 2GMr + Q^2(r) + a^2 = 0, \quad (10)$$

which depends on $Q(r)$ a function of r , and is different from the Kerr-Newman black hole, where Q is just a constant. The solution Eq. (10) can have either no roots (naked singularity), two roots (horizons) depending on the values of these parameters. It is difficult to solve the Eq. (10) analytically and hence we approach for numerical solutions. It is seen that Eq. (10) admits two horizons r_{EH}^- and r_{EH}^+ for suitable choice of parameters, which corresponds to two positive roots of Eq. (10), with r_{EH}^+ determines the event horizons and r_{EH}^- the Cauchy horizon. Further, it is worthwhile to mention that one can set parameters when r_{EH}^- and r_{EH}^+ are equal and we have an extremal black hole. We have plotted the event horizons in Fig. 2-3 for different values of mass M , charge Q , parameter β and spinning parameter a . Like, the Kerr-Newman black hole, the rotating spacetime (8) has two horizons, viz., the Cauchy horizon and the event horizon. The figures reveals that there exists set of values of parameters for which we have two horizons, i.e., a black hole with both inner and outer horizons. One can also find values of parameters for which one get an extremal black hole where the two horizons coincide. The region between the static limit surface and the event horizon is termed as quantum ergosphere, where it is possible to enter and leave again, and the object moves in the direction of the spin of black hole. We have numerically studied the horizon properties for nonzero values of a , β and Q (cf. Fig. 4) by solving Eq. (10). It turns out that the Born-Infeld parameter β makes a profound influence on the horizon structure when compared with the Kerr black hole. We find that for a given values of parameters β, Q , there exist extremal value of $a = a_E$ and $r = r_H^E$ such that for $a < a_E$, Eq. (10) admits two positive roots, which corresponds to respectively, a black hole has two horizons or black hole with both Cauchy and event horizons. We found no root at $a > a_E$ (naked singularity) (see Fig. 4), i.e., existence of a naked singularity. Further, one can find values of parameters for which these two horizons coincide and we get extremal black holes. Similarly, we have shown that for given values of parameters a, β , we get an extremal value of $Q = Q_E$, for which two horizons coincide and we get extremal black holes as shown

in Fig. 4. Interestingly, the value of Q_E decreases with increase in β .

Infinite red-shift surface or static limit surface. While in non-rotating black hole, in general, the horizon is also the surface where g_{tt} changes sign, in rotating Einstein-Born-Infeld, like Kerr-Newman, these surfaces do not coincide. The location of infinite redshift surface or static limit surface requires the coefficient of dt^2 to vanish, i.e., it must satisfy

$$r^2 - 2GMr + Q^2(r) + a^2 \cos^2(\theta) = 0. \quad (11)$$

Eq. (11) is solved numerically and the behavior of the static limit surface which is shown in Figs. 5 and 6. The Einstein-Born-Infeld metric (8) admits two static limit surfaces r_{SLS}^- and r_{SLS}^+ corresponding to two positive roots of Eq. (11) when the parameters M, Q, a , and β are chosen suitably (cf. Figs. 5 and 6). Interestingly the radius of the static limit surface decreases with increase in the value of parameter β . The static limit surface has similar extremal behavior which is depicted in the Figs. 5 and 6). Like any other rotating black hole, there is a region outside the outer horizon where $g_{tt} > 0$. The region, i.e. $r_{SLS}^+ < r < r_{EH}^+$ is called ergoregion, and its outer boundary $r = r_{SLS}^+$ is called the quantum ergosphere.

Null geodesics in Einstein-Born-Infeld black hole spacetime. Next, we turn our attention to the study the geodesic of a photon. We need to study the separability of the Hamilton-Jacobi equation using the approach due to Carter [19]. First, for generality we consider a motion for a particle with mass m_0 falling in the background of a rotating Einstein-Born-Infeld black hole. The geodesic motion for this black hole is determined by the following Hamilton-Jacobi equations

$$\frac{\partial S}{\partial \tau} = -\frac{1}{2}g^{\mu\nu} \frac{\partial S}{\partial x^\mu} \frac{\partial S}{\partial x^\nu}, \quad (12)$$

where τ is an affine parameter along the geodesics, and S is the Jacobi action. For this black hole background the Jacobi action S can be separated as

$$S = \frac{1}{2}m_0^2\tau - Et + L\phi + S_r(r) + S_\theta(\theta), \quad (13)$$

where S_r and S_θ are respectively functions of radial coordinate r and angle θ . Like the Kerr space-time, rotating Born-Infeld black hole also has two Killing vector fields due to the assumption of stationarity and axisymmetry of the space-time, which in turn guarantees the existence of two conserved quantities for a geodesic motion, viz. the energy E and the axial component of the angular momentum L . Thus, the constants m_0 , E , and L correspond to rest mass, conserved energy and rotation parameter related through $m_0^2 = -p_\mu p^\mu$, $E = -p_t$,

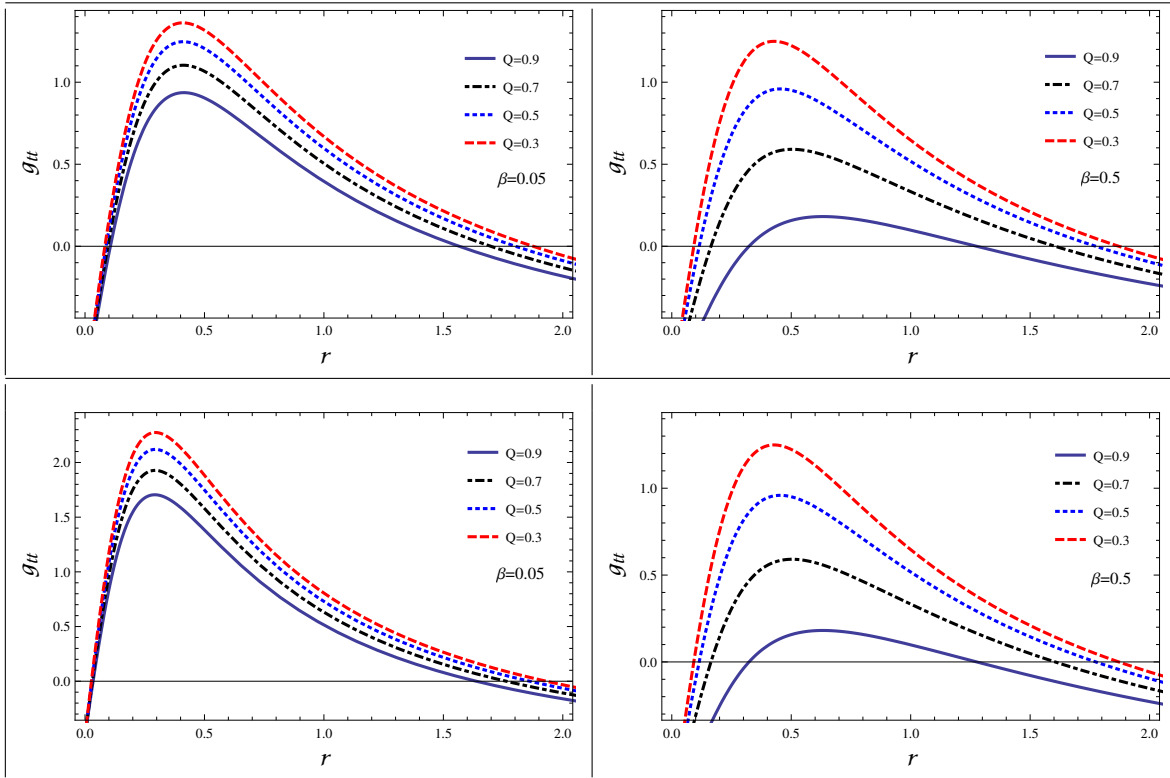


Fig. 5 Plots showing the radial dependence of g_{tt} component of metric tensor for the different values of Born-Infeld parameter β and electric charge Q (with $M = 1$). Top, left panel is for $\beta = 0.05$, $a = 0.45$ and $\alpha = \pi/6$. Top, right panel is for $\beta = 0.5$, $a = 0.45$ and $\alpha = \pi/6$. Bottom, left panel is for $\beta = 0.05$, $a = 0.45$ and $\alpha = \pi/3$. Bottom, right panel is for $\beta = 0.5$, $a = 0.45$ and $\alpha = \pi/3$.

and $L = p_\phi$. Obviously for a photon null geodesic, we have $m_0 = 0$, and from (12) we obtain the null geodesics in the form of the first-order differential equations

$$\rho^2 \frac{dt}{d\tau} = \frac{r^2 + a^2}{\Delta} [(r^2 + a^2)\mathcal{E} - a\mathcal{L}] + a(\mathcal{L} - a\mathcal{E} \sin^2 \theta), \quad (14)$$

$$\rho^2 \frac{d\phi}{d\tau} = \frac{a}{\Delta} [(r^2 + a^2)\mathcal{E} - a\mathcal{L}] + \left(\frac{\mathcal{L}}{\sin^2 \theta} - a\mathcal{E} \right), \quad (15)$$

$$\rho^2 \frac{dr}{d\tau} = \sqrt{\mathcal{R}}, \quad (16)$$

$$\rho^2 \frac{d\theta}{d\tau} = \sqrt{\Theta}, \quad (17)$$

where the functions $\mathcal{R}(r)$ and $\Theta(\theta)$ are defined as

$$\mathcal{R} = [(r^2 + a^2)\mathcal{E} - a\mathcal{L}]^2 - \Delta(\mathcal{K} + (\mathcal{L} - a\mathcal{E})^2), \quad (18)$$

$$\Theta = \mathcal{K} + \cos^2 \theta \left(a^2 \mathcal{E}^2 - \frac{\mathcal{L}^2}{\sin^2 \theta} \right).$$

Thus, we find that Hamilton-Jacobi Eq. (12), using (13), is separable due existence of \mathcal{K} namely Carter constant of separation. The above equations govern the light propagation in the Einstein-Born-Infeld black hole background. Obviously, for $Q = 0$, they are just the null

geodesic equations for the Kerr black hole. The constant $\mathcal{K} = 0$ is the necessary and sufficient condition for particles motion initially in the equatorial plane to remain their. Any particle which crosses the equatorial plane has $\mathcal{K} > 0$.

Effective potential. The discussion of effective potential is a useful tool for describing the motion of test particles. Further, we have to study radial motion of photon for determining the black hole shadow boundary. The radial equation for timelike particles moving along geodesic in the equatorial plane ($\theta = \pi/2$) is described by

$$\frac{1}{2} \dot{r}^2 + V_{eff} = 0, \quad (19)$$

with the effective potential

$$V_{eff} = - \frac{[E(r^2 + a^2) - La]^2 - \Delta(L - aE)^2}{2r^4}. \quad (20)$$

From the last expression (20) one can easily get the plots presented in Figs. 7 and 8. There we have considered photon motion around Einstein-Born-Infeld black hole for the different values of electric charge Q and parameter β . It is shown that with increasing electric charge Q or rotating parameter a particle is going to come closer to the central object.

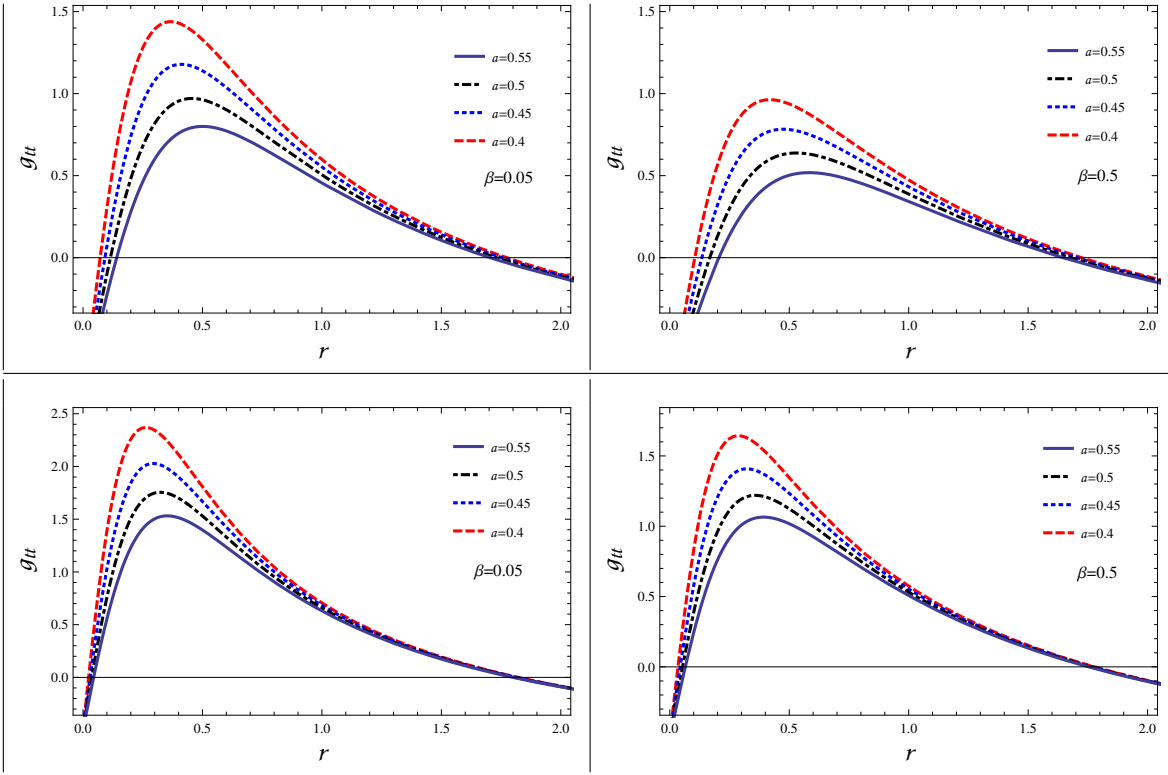


Fig. 6 Plots showing the radial dependence of g_{tt} component of metric tensor for the different values of parameter β and rotation parameter a (with $M = 1$). Top, left panel is for $\beta = 0.05$, $Q = 0.6$ and $\alpha = \pi/6$. Top, right panel is for $\beta = 0.5$, $Q = 0.6$ and $\alpha = \pi/6$. Bottom, left panel is for $\beta = 0.05$, $Q = 0.6$ and $\alpha = \pi/3$. Bottom, right panel is for $\beta = 0.5$, $Q = 0.6$ and $\alpha = \pi/3$.

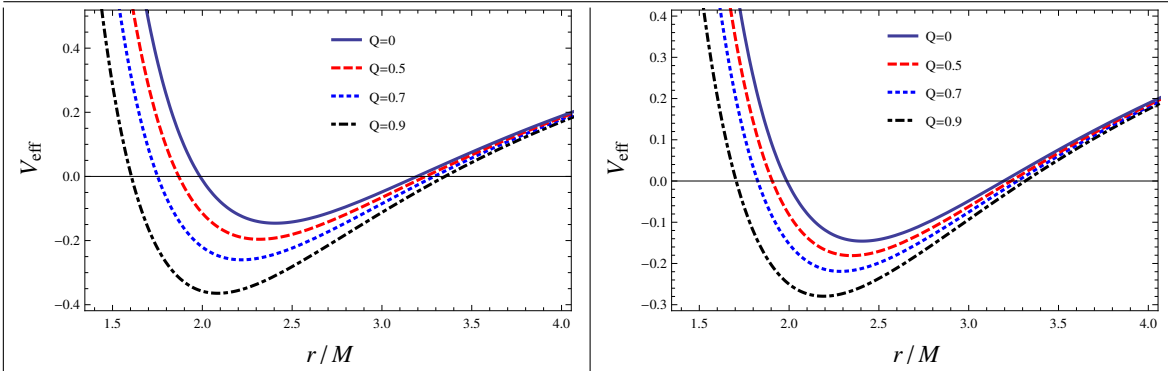


Fig. 7 The radial dependence of effective potential V_{eff} for the photon for the different values of electric charge Q . Left panel is for $\beta = 0.05$ and $a = 0.5$; right one is for $\beta = 0.5$ and $a = 0.5$.

3 Shadows of Einstein-Born-Infeld black holes

Now, it is general belief that a black hole, if it is in front of a bright background produced by far radiating object, will cast a shadow. The apparent shape of a black hole silhouette is defined by the boundary of the black and it was first studied by Bardeen [20]. The ability of very long baseline interferometry (VLBI) observation has been improved significantly at short wavelength which led to strong expectation that within few

years it may be possible to observe the direct image of the accretion flow around a black hole with a high resolution corresponding to black hole event horizon [21]. This may allow help us to test gravity in the strong field regime and investigate the properties of black hole candidates. The VLBI experiments is also looking for the shadow of a black hole, i.e. a dark area in front of a luminous background [20,22]. Hence, there is a significant attention towards study of black hole shadow and

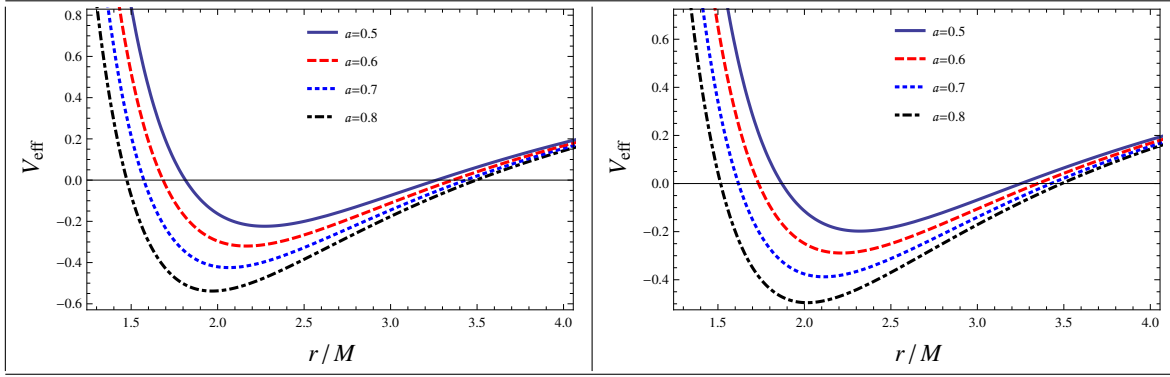


Fig. 8 The radial dependence of effective potential V_{eff} for the photon for the different values of rotation parameter a . Left panel is for $\beta = 0.05$ and $Q = 0.6$; right one is for $\beta = 0.5$ and $Q = 0.6$.

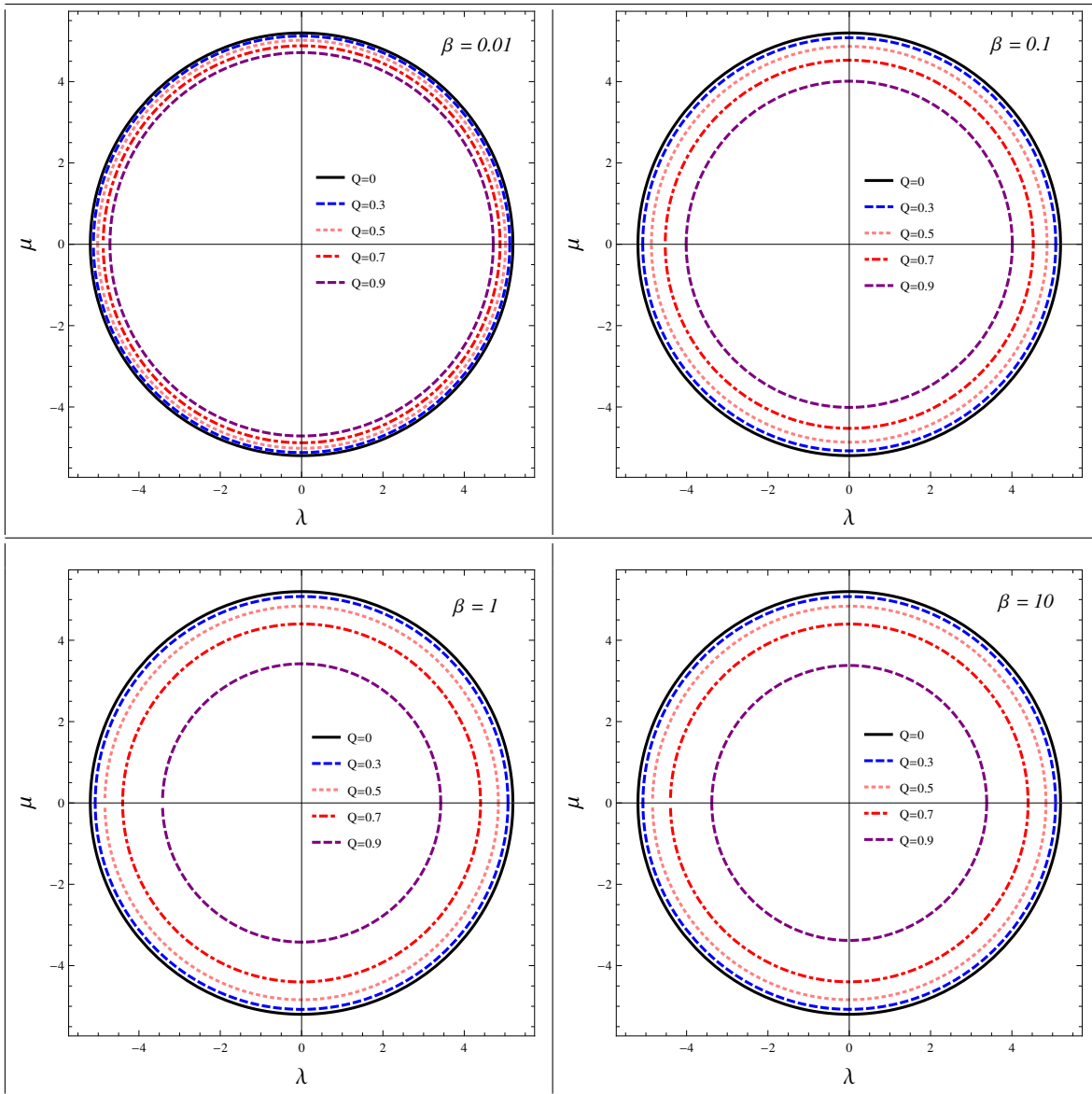


Fig. 9 Shadow of the black hole for the different values of electric charge Q . Top, left panel is for Born-Infeld parameter $\beta = 0.01$. Top, right panel is for Born-Infeld parameter $\beta = 0.1$. Bottom, left panel is for Born-Infeld parameter $\beta = 1$. Bottom, right panel is for Born-Infeld parameter $\beta = 10$ (with $M = 1$ and $a = 0$).

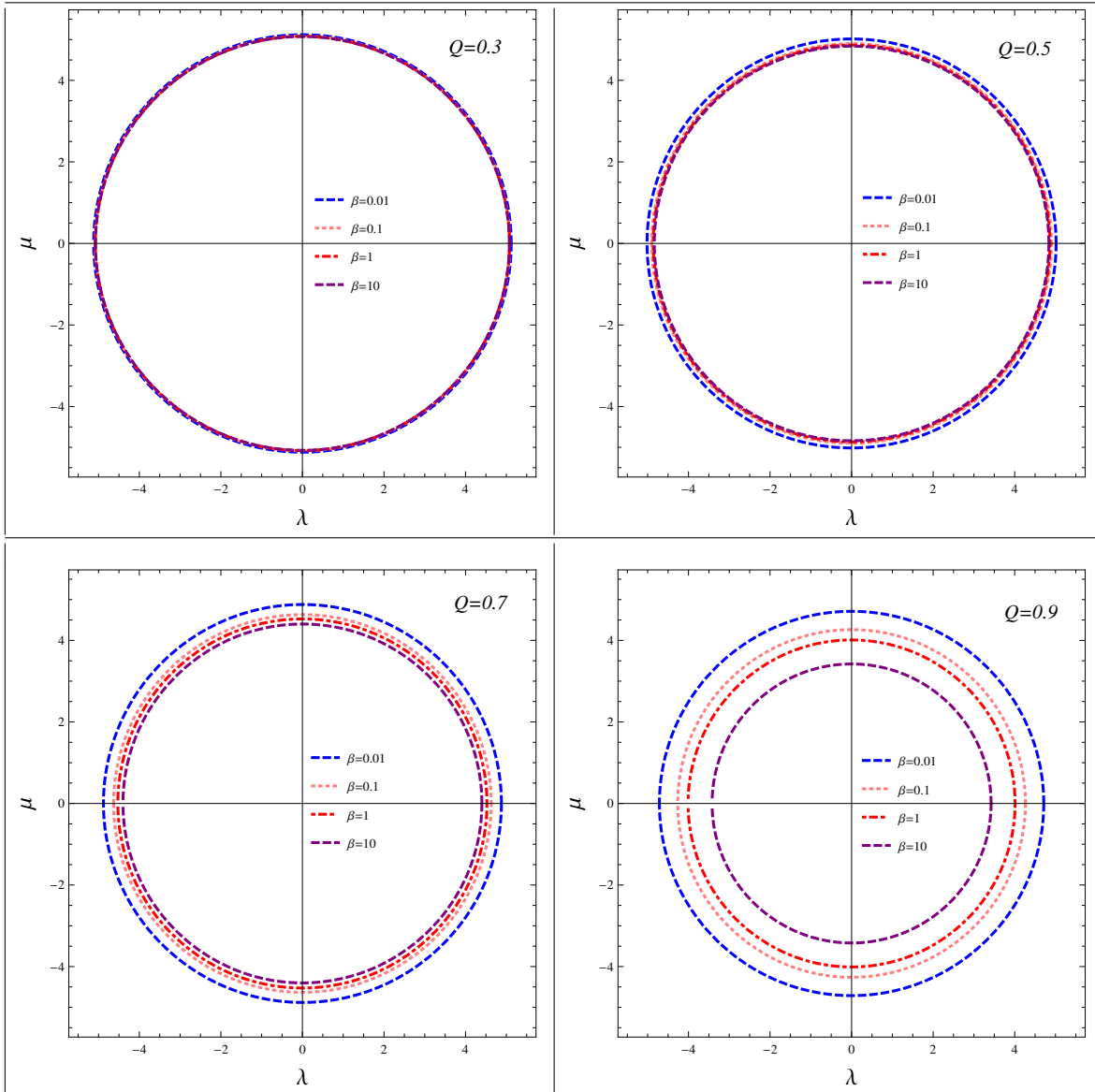


Fig. 10 Shadow of the black hole for the different values of Born-Infeld parameter β . Top, left panel is for electric charge $Q = 0.3$. Top, right panel is for electric charge $Q = 0.5$. Bottom, left panel is for electric charge $Q = 0.7$. Bottom, right panel is for electric charge $Q = 0.9$ (with $M = 1$ and $a = 0$).

it has become a quite active research field [15] (for a review, see [23]). For the Schwarzschild black hole the shadow of the black hole is a perfect circle [23], and that enlarges in the case of Reissner-Nordström black hole [24]. Here, we plan to discuss the shadow of the Einstein-Born-Infeld black hole, and we shall confine to non-rotating ($a = 0$) case. It is possible to study equatorial orbits of photon around Einstein-Born-Infeld black holes via the effective potential. It is generally known, that the photon orbits are of three types: scattering, falling and unstable [25]. *The falling orbits* are due to the photons arriving from infinity cross the horizon and fall down into the black hole, they have more en-

ergy than barrier of the effective potential. The photons arriving from infinity move along *the scattering orbits* and come back to infinity, and with energy less than the barrier of the effective potential. Finally, the maximum value of the effective potential separates the captured and the scattering orbits and defines unstable orbits of constant radius (it is circle located at $r = 3M$ for the Schwarzschild black hole) which is responsible for the apparent silhouette of a black hole. Distinct observer will be able to see only the photons scattered away from the black hole, while those captured by the black hole will form a dark region. If the black hole appears between a light source and a distant observer, the photons

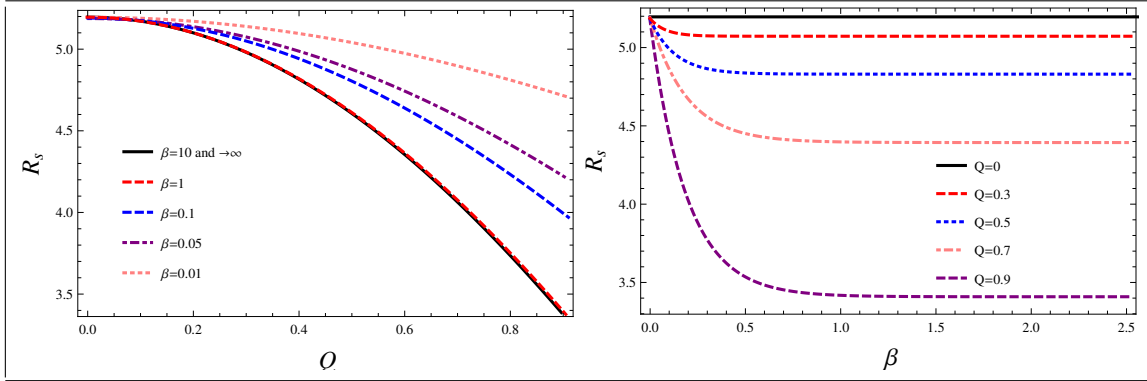


Fig. 11 The dependence of observable radius of black hole shadow R_s from the electric charge Q and Born-Infeld parameter β . Left panel is showing graphs for the different values of Born-Infeld parameter β . The right panel is showing graphs for the different values of electric charge Q .

with small impact parameters fall into the black hole and form a dark zone in the sky which is usually termed as black hole shadow. We consider the following series expansion

$$\frac{4Q^2}{3} F\left(\frac{1}{4}, \frac{1}{2}, \frac{5}{4}, -\zeta^2(r)\right) \approx \frac{4Q^2}{3} \left(1 - \frac{\zeta^2(r)}{10}\right) + \mathcal{O}\left(\frac{1}{\beta^4}\right). \quad (21)$$

Also, all the higher order terms from onwards have been dropped out from the series expansion of $F\left(\frac{1}{4}, \frac{1}{2}, \frac{5}{4}, -\zeta^2(r)\right)$ which yields

$$Q^2(r) \approx \frac{2\beta^2 r^4}{3} \left(1 - \sqrt{1 + \zeta^2(r)}\right) + \frac{4Q^2}{3} \left(1 - \frac{\zeta^2(r)}{10}\right) + \mathcal{O}\left(\frac{1}{\beta^4}\right), \quad (22)$$

and accordingly Δ is also modified and we denote the new Δ as Δ' , which reads

$$\Delta' = -2 + \frac{8Q^2\zeta^2(r)}{15r} + \frac{4Q^2}{3r\sqrt{1 + \zeta^2(r)}} + 2r - \frac{8\beta^2 r^3}{3} \left(-1 + \sqrt{1 + \zeta^2(r)}\right). \quad (23)$$

Henceforth, all our calculations are valid up to $\mathcal{O}\left(\frac{1}{\beta^4}\right)$ only. An effective potential for the photon attains a maximum, goes to negative infinity beneath the horizon, asymptotically goes to zero at $r \rightarrow \infty$. In the standard Schwarzschild black hole, the maximum of the effective potential occurs at $r = 3M$, which is also the location of the unstable orbit and no minimum. The behavior of effective potential as a function of radial coordinate r for different values of parameter β , rotation parameter a and Q are depicted in Figs. 7 and 8. It is observed that the potential has a minimum which imply the presence of stable circular orbits. The apparent shape of the black hole is obtained by observing the closed orbits around the black hole governed by three

impact parameters, which are functions of E , L_ϕ and L_ψ and the constant of separability \mathcal{K} . The equations determining the unstable photon orbits, in order to obtain the boundary of shadow of the black holes, are Eq.(19) or

$$R(r) = 0 = \partial R(r)/\partial r$$

which are fulfilled by the values of the impact parameters

$$\xi = \frac{(r^2 + a^2)\Delta' - 4r\Delta}{\Delta'a}, \quad (24)$$

and

$$\eta = \frac{16\Delta r^2 a^2 - \left((r^2 + a^2)\Delta' - 4r\Delta - a\Delta'\right)}{(\Delta'a)^2}, \quad (25)$$

that determine the contour of the shadow. whereas the parameter ξ and η satisfy

$$\xi^2 + \eta = \frac{4A\left(\frac{8Q^2 r_0 \zeta^2(r_0)}{15} - \frac{8Q^2 r_0}{3} + \frac{2Q^2 r_0}{3\sqrt{1 + \zeta^2(r_0)}} + 3r_0^2 - r_0^3\right) - 1 + \frac{4Q^2 \zeta^2(r_0)}{15r_0} + \frac{2Q^2}{3r_0\sqrt{1 + \zeta^2(r_0)}} + r_0 - \frac{4}{3}\beta^2 r_0^3 \left(-1 + \sqrt{1 + \zeta^2(r_0)}\right) + \frac{60\beta^2 r_0^4 B}{C} + \mathcal{O}(a^2)}{\quad} \quad (26)$$

with

$$A = -1 + \frac{4Q^2 \zeta^2(r_0)}{15r_0} + \frac{2Q^2}{3r_0\sqrt{1 + \zeta^2(r_0)}} - r_0 - \frac{4}{3}\beta^2 r_0^3 \left(-1 + \sqrt{1 + \zeta^2(r_0)}\right) \quad (27)$$

$$B = 6Q^6 - 14\beta^2 Q^4 r_0^4 + 15\beta^2 Q^2 r_0^5 - 10\beta^4 Q^2 r_0^8 + 15\beta^4 r_0^9 + 10\beta^6 r_0^{12} - 10\beta^6 r_0^{12} \sqrt{1 + \zeta^2(r_0)} \quad (28)$$

$$C = 4\beta Q^4 \sqrt{1 + \zeta^2(r_0)} + 20\beta^5 r_0^8 \left(-1 + \sqrt{1 + \zeta^2(r_0)}\right) - 5\beta^3 r_0^4 \left(2Q^2 - 3r_0(r_0 - 1)\sqrt{1 + \zeta^2(r_0)}\right)^2 \quad (29)$$

The shadow of Einstein-Born-Infeld black holes may be determined through virtue of the above equation. In order to study the shadow of Einstein-Born-Infeld black hole, it is necessary to introduce the celestial coordinates according to [26]

$$\lambda = \lim_{r_0 \rightarrow \infty} \left(-r_0^2 \sin \theta_0 \frac{d\phi}{dr} \right), \quad (30)$$

and

$$\mu = \lim_{r_0 \rightarrow \infty} r_0^2 \frac{d\theta}{dr}, \quad (31)$$

The celestial coordinates can be rewritten as

$$\lambda = -\xi \csc \theta_0, \quad (32)$$

$$\mu = \pm \sqrt{\eta + a^2 \cos^2 \theta_0 - \xi \cot^2 \theta_0}, \quad (33)$$

and formally coincide with that for the Kerr black hole. However in reality ξ and η are different for the Einstein-Born-Infeld black hole. The celestial coordinate in the equatorial plane ($\theta_0 = \pi/2$), where observer is placed, becomes

$$\lambda = -\xi, \quad (34)$$

and

$$\mu = \pm \sqrt{\eta}, \quad (35)$$

The apparent shape of the Einstein-Born-Infeld black hole shadow can be obtained by plotting λ vs μ as

$$\lambda^2 + \mu^2 = \xi^2 + \eta, \quad (36)$$

which suggests that the shadow of Einstein-Born-Infeld black holes in (λ, μ) space is a circle with radius of the quantity defined by the right hand side of equation (26). Thus, the shadow of the black hole depends on the electric charge Q and Born-Infeld parameter β both. These are depicted in Figs. 9 and 10 for the different values of these parameters.

In the limit, $\beta \rightarrow \infty$, the above expression reduces to

$$\xi^2 + \eta = \lambda^2 + \mu^2 = \frac{2r_0^2(r_0^2 - 3) + 4r_0Q^2}{(r_0 - 1)^2}. \quad (37)$$

which is same as that for Reissner-Nordstrom black hole. In addition, if we switch off electric charge $Q = 0$, one gets expression for Schwarzschild case, which reads as

$$\xi^2 + \eta = \lambda^2 + \mu^2 = \frac{2r_0^2(r_0^2 - 3)}{(r_0 - 1)^2}. \quad (38)$$

In order to extract more detailed information from the shadow of the Einstein-Born-Infeld black holes, we must create the observables. In general, there are two observable parameters as radius of shadow R_s and distortion parameter δ_s [27]. For non-rotating black hole

there is only single parameter R_s which corresponds to radius of reference circle. From Figs. 9 and 10 one can get numerical value for the radius of black hole shadow which is clearly shown in Fig.11.

At high energies the absorption cross section of a black hole has variation around a limiting constant value and for the distant observer placed at infinity the black hole shadow is responsible to its high energy absorption cross section. For a black hole having a photon sphere, the limiting constant value coincides with the geometrical cross section of the photon sphere [28].

4 Emission energy of rotating Einstein-Born-Infeld black holes

For completeness of our research here we investigate rate of the energy emission from the Einstein-Born-Infeld black hole with the help of

$$\frac{d^2 E(\omega)}{d\omega dt} = \frac{2\pi^2 \sigma_{lim}}{\exp \omega/T - 1} \omega^3, \quad (39)$$

where $T = \kappa/2\pi$ is the Hawking temperature, and κ is the surface gravity. At outer horizon the temperature T is equal to

$$T = \frac{2Q^4 \sqrt{1 + \zeta^2(r_+)} - 2\beta^2 Q^2 r_+^4 \left(1 + 2\sqrt{1 + \zeta^2(r_+)} \right)}{12\beta^2 \pi r_+^5 (a^2 + r_+^2) \sqrt{1 + \zeta^2(r_+)}} + \frac{3r_+^4 \beta^2 D}{12\beta^2 \pi r_+^5 (a^2 + r_+^2) \sqrt{1 + \zeta^2(r_+)}} , \quad (40)$$

where

$$D = -a^2 \sqrt{1 + \zeta^2(r_+)} + r_+^2 (\sqrt{1 + \zeta^2(r_+)} + 2\beta^2 r_+^2 (\sqrt{1 + \zeta^2(r_+)} - 1)) \quad (41)$$

The limiting constant σ_{lim} defines the value of the absorption cross section vibration of for a spherically symmetric black hole:

$$\sigma_{lim} \approx \pi R_s^2. \quad (42)$$

Consequently according to [29] we have

$$\frac{d^2 E(\omega)}{d\omega dt} = \frac{2\pi^3 R_s^2}{e^{\omega/T} - 1} \omega^3.$$

The dependence of energy emission rate from frequency for the different values of electric charge Q and parameter β is shown in Fig. 12. One can see that with the increasing electric charge Q or parameter β the maximum value of energy emission rate decreases, caused by horizon area decrease.

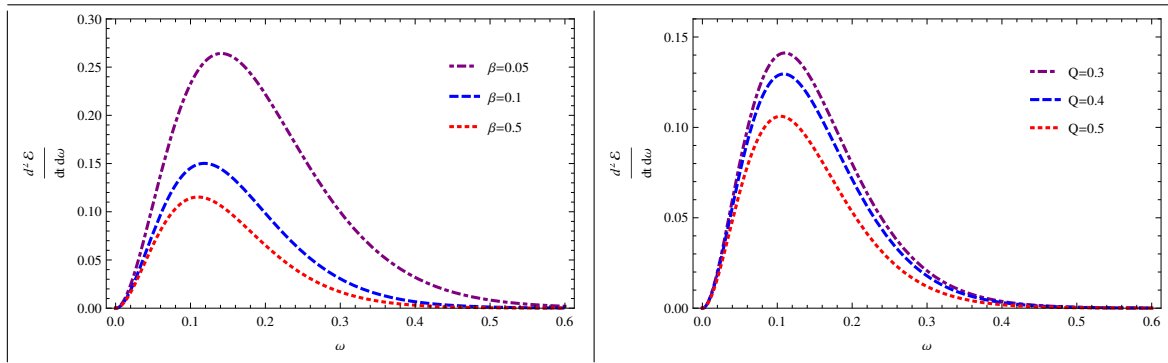


Fig. 12 Energy emission of black hole in Einstein-Born-Infeld gravity. Left panel is for electric charge $Q = 0.5$ and right panel is for Born-Infeld parameter $\beta = 0.05$.

5 Conclusion

In recent years the Born-Infeld action has received a significant attention to the development of superstring theory, where it has been demonstrated that the Born-Infeld action naturally arises in string-generated corrections when one considers an open superstring. This leads to interest in extending the Reissner-Nordstrom black hole solutions in Einstein-Maxwell theory to the charged black hole solution in Einstein-Born-Infeld theory [5]. In view of this, we have investigated the horizon structure of the charged rotating black hole solution in Einstein-Born-Infeld theory, and explicitly discuss the effect of the Born-Infeld parameter β into event horizon and optical properties of black hole. Further, this rotating Einstein-Born-Infeld black hole solution generalizes both Reissner-Nordstrom ($\beta \rightarrow \infty$ and $a = 0$) and Kerr-Newman solutions ($\beta \rightarrow \infty$). Interestingly, it turns out that for given values of parameters $\{M, Q, \beta\}$, there exists $a = a_E$ for which the solution (8) can be an extremal black hole, which decreases with increase in the parameter β . Further, we have also analyzed infinite red-shift surfaces, ergo-regions, energy emission and Hawking temperature of the rotating Einstein-Born-Infeld black hole. The Einstein-Born-Infeld black hole's horizon structure has been studied for the different values of electric charge Q and Born-Infeld parameter β , which explicitly demonstrates that outer (inner) horizon radius decreases (increases) with increase in the electric charge Q and Born-Infeld parameter β . We have done our calculations numerically as it is difficult to solve the analytical solution and found that the obtained results are different from the Kerr-Newman case due to non-zero Born-Infeld parameter β . It is well known that a black hole can cast a shadow as an optical appearance due to its strong gravitational field. Using the gravitational lensing effect, we have also investigated the shadow cast by the non-rotating ($a = 0$)

Einstein-Born-Infeld black hole and demonstrated that the null geodesic equations can be integrated that allows us investigate the shadow cast by a black hole which is found to be a dark zone covered by a circle. The shadow is slightly smaller and less deformed than that for its Reissner-Nordstrom counterpart. Further, the shadow of the Einstein-Born-Infeld black hole is concentric circle. In addition, the Born-Infeld parameter β also changes the shape of the black hole's shadow. In considered case of the nonrotating black hole only a radius of the shadow is observable parameter and from the numerical calculations we have easily got the value of the radius of the black hole shadow. The effective potential for geodesic motion of the photon around rotating Einstein-Born-Infeld black hole has been studied for the different values of the electric charge and spin parameter of the black hole. With increasing either rotation parameter or electric charge of black hole particle is moving closer to the central object. Hence, circular orbit of the photon becomes closer to the center of rotating Einstein-Born-Infeld black hole. It will be of interest to discuss energy extraction from rotating Einstein-Born-Infeld black hole, as the ergo-region is influenced by the Born-Infeld parameter and hence may enhance the efficiency of Penrose process. This and related work are the subject of forthcoming papers. Finally, in particular our results in the limit $\beta \rightarrow \infty$, reduced exactly to Kerr-Newman black hole, and to Kerr black when $Q(r) = 0$.

Acknowledgments

BA thanks the TIFR and IUCAA for the warm hospitality during his stay in Mumbai and Pune, India. This research is partially supported by the projects F2-FA-F113, FE2-FA-F134 of the Uzbekistan Academy of Sciences and by the ICTP through the OEA-PRJ-29 and OEA-NET-76 grants. BA acknowledges the TWAS As-

sociateship grant. Support from the Volkswagen Stiftung (Grant 86 866) is also acknowledged. SGG thanks IUCAA for hospitality while part of the work was being done, and to SERB-DST, Government of India for Research Project Grant NO SB/S2/HEP-008/2014.

References

1. M. Born and L. Infeld, Proc. R. Soc.(London) **144**, 425 (1934).
2. B. Hoffmann, Phys. Rev. **47**, 877 (1935).
3. E. S. Fradkin and A. A. Tseytlin, Phys. Lett. B **163**, 123 (1985); E. Bergshoeff, E. Sezgin, C. N. Pope, and P. K. Townsend, Phys. Lett. B **188**, 70 (1987); R. R. Metsaev, M. A. Rahmanov, and A. A. Tseytlin, Phys. Lett. B **193**, 207 (1987).
4. E. S. Fradkin and A. A. Tseytlin, Phys. Lett. B **163**, 123 (1985).
5. J.A. Feigenbaum, Phys. Rev. D **58**, 124023 (1998); J.A. Feigenbaum, P.O. Freund, M. Pigli, Phys. Rev. D **57**, 4738 (1998). D. Comelli, Phys. Rev. D **72**, 064018 (2005); D. Comelli, A. Dolgov, JHEP **0411**, 062 (2004); J.A. Nieto, Phys. Rev. D **70**, 044042 (2004); M.N.R. Wohlfarth, Class. Quant. Grav. **21**, 1994 (2004).
6. M. Demianski, 1986 Found. Phys. **16**, 187; H. dOliveira, Class. Quant. Grav. **11** 1469 (1994); S. Fernando and D. Krug, Gen. Rel. Grav. **35**, 129 (2003).
7. R. Linares, M. Maceda, and D. M. Carbajal arXiv:gr-qc/1412.3569 v1.
8. R. P. Kerr, Phys. Rev. Lett. D **11**, 237 (1963).
9. E. T. Newman and A. I. Janis, J. Math. Phys. **6**, 915 (1965).
10. D. J. Cirilo Lombardo, Class. Quant. Grav. **21**, 1407 (2004) [gr-qc/0612063].
11. A. A. Shoom, Phys. Rev. D **91**, 064030 (2015); A. A. Shoom, Phys. Rev. D **91**, 024019 (2015); S. Abdolrahimi and A. A. Shoom, Phys. Rev. D **83**, 104023 (2011). G. G. Sushant and M. Amir, arXiv:1506.04382 (2015).
12. J. P. Luminet, Astron.Astrophys. **75**, 228 (1979).
13. J. Schee and Z. Stuchlik, Int. Jour. Mod. Phys. D **18**, 983 (2009). Z. Stuchlik and J. Schee, Class. and Quant. Grav., **27**, 21, (2010). Z. Stuchlik and J. Schee, Int. Jour. of Mod. Phys D. **24**, 2,1550020(2015). Z. Stuchlik and J.Schee, Class. and Quant. Grav., **29**, 6, 065002(2012).
14. K. S. Virbhadra, Phys. Rev. D **79**, 083004 (2009). K. S. Virbhadra and C. R. Keeton, Phys. Rev. D **77**, 124014 (2008). K. S. Virbhadra and G. F. Ellis, Phys. Rev. D **65**, 103004 (2008).
15. L. Amarilla and E. F. Eiroa, Phys. Rev. D, **87**, 044057 (2013); A. de Vries, Class. Quant. Grav. **17**, 123 (2000). H. Falcke and S. B. Markoff, Classical and Quantum Gravity, **30**, 244003 (2013); C. Bambi and N. Yoshida, Classical Quantum Gravity **27**, 205006 (2010). A. Grenzebach, V. Perlick, C. Lammerzahl, and S. Reimers, Phys. Rev. D **89**, 124004 (2014). A. Abdujabbarov, F. Atamurotov, Y. Kucukakca, B. Ahmedov and U. Camci, Astrophys. Space Sci. **344**, 429 (2013); F. Atamurotov, A. Abdujabbarov and B. Ahmedov, Phys. Rev. D **88**, 064004 (2013); F. Atamurotov, A. Abdujabbarov and B. Ahmedov, Astrophys. Space Sci. **348**, 179 (2013); U. Papnoi, F. Atamurotov, S. G. Ghosh, B. Ahmedov, Phys. Rev. D, **90**, 024073 (2014); A. F. Zakharov, A. A. Nucita, F. DePaolis, and G. Ingrosso, New Astron. **10**, 479 (2005); V. K. Tinchev and S. S. Yazadjiev, Int. J. Mod. Phys. D **23**, 1450060 (2014); P. G. Nedkova, V. K. Tinchev, and S. S. Yazadjiev, Phys. Rev. D **88**, 124019 (2013); A. F. Zakharov, Phys. Rev. D **90**, 062007 (2014); A. F. Zakharov, arXiv:1407.2591 (2014); C. Bambi, arXiv:1409.0310 (2014); T. Johannsen, Astrophys. J. **777**, 17 (2013).
16. A. A. Abdujabbarov, L. Rezzolla and B. J. Ahmedov, arXiv:1503.09054 (2015).
17. G. W. Gibbons and D. A. Rasheed, Nucl. Phys. B **454**, 185 (1995); G. W. Gibbons and D. A. Rasheed, Nucl. Phys. B **476**, 515 (1996); D. Chruscinski, Phys. Rev. D **62**, 105007 (2000); D. Sorokin, hep-th/9709190 .
18. M. Abramowitz, I. A. Stegun, Handbook of Mathematical Functions (Dover, New York, 1972).
19. B. Carter, Phys. Rev. **174** 1559 (1968).
20. J. M. Bardeen, in Black holes, Proceedings of the Les Houches Summer School, Session 215239, edited by C. De Witt and B. S. De Witt (Gordon and Breach, New York, 1973).
21. S. Doeleman et. al. Nature **455** 78 (2008); S. Doeleman, et. al. arXiv:0906.3899 (2009).
22. H. Falcke, F. Melia and E. Agol, 2000 Astrophys. J. **528**, L13 (arXiv:astro-ph/9912263)
23. V. Bozza, Gen. Relativ. Gravit. **42**, 2269 (2010).
24. E. F. Eiroa, G. E. Romero, and D. F. Torres, Phys. Rev. D **66**, 024010 (2002).
25. C. Bambi and K. Freese, Phys. Rev.D **79**, 043002 (2009); C. Bambi and N. Yoshida, Class. Quant. Grav. **27**, 205006 (2010).
26. S. E. Vazquez and E. P. Esteban, Nuovo Cim. **119**, 489 (2004).
27. K. Hioki and K. I. Maeda, Phys. Rev. D **80**, 024042 (2009).
28. C. W. Misner, K.S. Thorne, and J.A. Wheeler, *Gravitation* (W.H. Freeman, San Francisco, 1973).
29. S. W. Wei and Y. X. Liu, JCAP **1311**, 063 (2013).